Journal of Power Sources 258 (2014) 424–433

Contents lists available at ScienceDirect

Journal of Power Sources

journal homepage: www.elsevier.com/locate/jpowsour

# Electrochemical performance of V-doped spinel $Li_4Ti_5O_{12}$/C composite anode in Li-half and $Li_4Ti_5O_{12}$/$LiFePO_4$-full cell

Chun-Chen Yang [a,b,*], Huai-Chou Hu [a], S.J. Lin [b], Wen-Chen Chien [a,b]

[a] Department of Chemical Engineering, Ming Chi University of Technology, New Taipei City 243, Taiwan, ROC
[b] Battery Research Center of Green Energy, Ming Chi University of Technology, New Taipei City 243, Taiwan, ROC

## HIGHLIGHTS

- This work reports the preparation of a V-doped $Li_4Ti_5O_{12}$/C by a solid-state method.
- $Li_4Ti_5O_{12}$/$LiFePO_4$ full cell was investigated and exhibited excellent performance.
- $Li_4Ti_{4.95}V_{0.05}O_{12}$/C and $LiFePO_4$ materials are good candidates for Li-ion battery.

## GRAPHICAL ABSTRACT

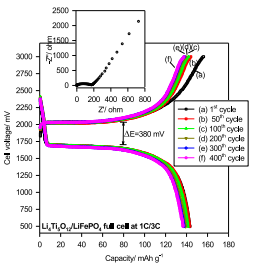


## ARTICLE INFO

*Article history:*
Received 11 December 2013
Received in revised form
9 January 2014
Accepted 20 January 2014
Available online 22 February 2014

*Keywords:*
Lithium titanium oxide/C composite
Anode materials
Lithium iron phosphate
Vanadium
Doping

## ABSTRACT

This work reports the preparation of a V-doped $Li_4Ti_5O_{12}$/C (donated as V-doped LTO/C) composite material, applying a solid-state method. Both metal doping and carbon coating are applied on the $Li_4Ti_5O_{12}$ material, enhancing its rate capability and cycle stability. Furan polymer is used as a carbon source, and vanadium (V) is selected as a dopant. The properties of the materials are examined by X-ray diffraction (XRD), micro-Raman, scanning electron microscopy (SEM), high-resolution transmission microscopy (HR-TEM), the AC impedance method, and the galvanostatic charge/discharge method. For comparison, $Li_4Ti_5O_{12}$/C composite materials with and without V doping are also examined. The $Li_4Ti_{4.90}V_{0.10}O_{12}$/C composite material achieves discharge capacities of 165.59 and 76.76 mAh $g^{-1}$ at a 0.2/1C and 0.2/20C rate, respectively. A $Li_4Ti_5O_{12}$/$LiFePO_4$ full cell (LTO capacity-limited) is constructed and investigated. The full cell exhibits discharge capacities of 181, 178, 167, 142, 110, and 78 mAh $g^{-1}$ at 0.2, 0.5, 1, 3, 5, and 10C, respectively. We determine that the $Li_4Ti_{4.95}V_{0.05}O_{12}$/C composite anode is an outstanding candidate for application in high-power Li-ion batteries.



## 1. Introduction

Because of their high energy density, low cost, and high-rate capability, lithium-ion (Li-ion) batteries are used in cell phones, laptop computers, digital cameras, renewable energy storage, and smart grid applications. For hybrid electric vehicle (HEV) or electric vehicle (EV) applications, Li-ion batteries must be charged and discharged quickly, and therefore, the electrodes have to work at a high rate and maintain an excellent capacity and cycling stability. Graphite [1], mesocarbon microbeads (MCMB) [2], and vapor-growth carbon fiber (VGCF) [3] are some conventional anode materials. Spinel $Li_4Ti_5O_{12}$ [4–24] (denoted as LTO) is a prospective anode material for advanced Li-ion batteries. Spinel $Li_4Ti_5O_{12}$ shows many advantages when compared with currently used graphite materials. It has excellent electrochemical reversibility and thermodynamic stability, but without any structural or volume

* Corresponding author. Department of Chemical Engineering, Ming Chi University of Technology, New Taipei City 243, Taiwan, ROC.
*E-mail address:* ccyang@mail.mcut.edu.tw (C.-C. Yang).

http://dx.doi.org/10.1016/j.jpowsour.2014.01.130
0378-7753/

change during the charge/discharge process (a so-called zero strain material) [4], it offers a stable working voltage of approximately 1.55 V (vs. $Li/Li^+$), and can accommodate 3 Li ions with a theoretical capacity of 175 mAh $g^{-1}$ [6]. A voltage of 1.55 V is above the reduction potential of electrolyte solvents, but is not high enough to form a solid-electrolyte interface (SEI) film. Thus, the formation of Li dendrites can be prevented. However, the electronic structure of $Li_4Ti_5O_{12}$ is characterized by empty Ti 3d-states with a band gap energy of 2–3eV, giving it an insulating property. Therefore, the low electron conductivity of $Li_4Ti_5O_{12}$ ($\sigma_e = 10^{-13}$ S $cm^{-1}$) [7,8] leads to capacity-fading and low-rate capability. This drawback may hinder its mass production and application in Li-ion batteries for EV. Several methods have been proposed to solve the conductivity problem [9–23], including new preparation methods, e.g., sol-gel [9,14], spray pyrolysis [11], and solid state method [10]), doping with supervalent metal ions, e.g., Ti [15], Mn [15], Al [16], Mg [17], Nb [18], Zr [19], V [22,23], Na [24], Zn [25], La [26], Mo [27], and incorporating high-conductivity materials (e.g., carbon [14], carbon nanotubes, and graphene [9]) to the LTO. Nevertheless, few researchers have extended the discharge voltage of metal-doped LTO to 0.5 V or near 0 V to increase its discharge rate and capacity [20,21]. Some studies have investigated the application of LTO in $Li_4Ti_5O_{12}/LiFePO_4$ [28], $Li_4Ti_5O_{12}/LiNi_{1/3}Co_{1/3}Mn_{1/3}O_2$ [29], and $Li_4Ti_5O_{12}/LiNi_{0.5}Mn_{1.5}O_4$ full cells [30]. These reports indicated that the LTO anode has high-power capability and long-term cycling stability.

In this study, we prepared V-doped $Li_4Ti_5O_{12}$/C composite materials, using a solid-state method. Furan polymer was used as the carbon source. We investigated the effects of V doping and the residual carbon content on the characteristic properties and electrochemical performances of the materials. The characteristic properties of V-doped $Li_4Ti_5O_{12}$/C materials were examined by X-ray diffraction (XRD), micro-Raman spectroscopy, scanning electron microscopy (SEM), high-resolution transmission microscopy (HR-TEM), elemental analysis (EA), and micro-Raman spectroscopy. The electrochemical performances of V-doped $Li_4Ti_5O_{12}$/C electrodes were examined using an automatic galvanostatic charge/discharge unit and a cyclic voltammetry method. We constructed and evaluated a $Li_4Ti_5O_{12}/LiFePO_4$ (donated as LTO/LFP full cell), and the capacity is limited by LTO anode. We also studied the electrochemical properties of the LTO/LFP full cell in detail. Our results indicated that the LTO/LFP cell exhibited a superior high-rate capability and cycling stability, as compared with other cells.

## 2. Experimental

### 2.1. Preparation of $Li_4Ti_5O_{12}$/C composite materials

The novel $Li_4Ti_5O_{12}$/C composite materials were prepared using a solid-state method. The appropriate quantities of nano-sized $TiO_2$ (P90 Cabot), $Li_2CO_3$ (Aldrich), and Furan polymer, as the starting materials, were mixed in ethanol, and then ball-milled for 4 h in a planetary miller with a ball/reactant weight ratio of 5:1, at a rotation speed of 300 rpm. The added carbon source was maintained at 5 wt.%. The ball-milled precursor mixture was pre-sintered at 350 °C for 4 h, and then sintered at 700 °C, 800 °C, and 850 °C for 12 h in air.

### 2.2. Material characterization

The crystal structures of the $Li_4Ti_5O_{12}$/C composite samples were examined using an X-ray diffraction (XRD) spectrometer (Philip, X'pert Pro System). Surface morphology was revealed using a scanning electron microscope (SEM, Hitachi). The morphology of the carbon residue was observed using a high-resolution transmission electron microscope (HR-TEM, JEOL 2010F). Micro-Raman spectra were recorded on a confocal micro-Renishaw with a 632-nm He–Ne laser excitation. The carbon residual content in the sample was determined using an elemental analyzer (Perkin Elmer 2400). A suitable amount as-prepared LTO/C powders plus 3%PVDF binder was mixed and fabricated to form a pellet by a stainless die and 10 ton press. The electrical conductivity measurement was made on LTO/C pellet via AC impedance method. The LTO/C pellet was clamped between stainless steel (SS304), ion-blocking electrodes, each of surface area 1.32 $cm^2$, in a spring-loaded glass holder. The AC impedance measurements were carried out using an Autolab PGSTAT-30 equipment (Eco Chemie B.V., Netherlands). The AC spectra in the range of 100 kHz to 100 Hz at an excitation signal of 5 mV were recorded. The bulk resistance associated the pellet conductivity was determined from the high-frequency intercept of the impedance with real axis. Taking into account the thickness of the pellet, the electrical conductivity ($\sigma_e$) was calculated from the $R_b$ value, according to the equation: $\sigma_e = L/R_b \cdot A$, where $\sigma_e$ is the electrical conductivity of the pellet sample (S $cm^{-1}$), $L$ is the thickness (cm) of the pellet, $A$ is the cross-sectional area of the blocking electrode ($cm^2$), and $R_b$ is the bulk resistance (ohm) of the pellet sample. All LTO/C samples were examined at least three times. The electrical conductivity of the composite samples was measured using the AC impedance method (AutoLab, Eco Chemi PGSTAT 30).

### 2.3. Electrochemical performance measurements of the $Li_4Ti_5O_{12}$/C anode

The electrochemical performance of the $Li_4Ti_5O_{12}$/C composite battery was measured using a 2-electrode system (CR 2032 coin cell assembled in an argon-filled glove box). The $Li_4Ti_5O_{12}$/C and V-doped $Li_4Ti_5O_{12}$/C composite electrodes were prepared by mixing active $Li_4Ti_5O_{12}$/C materials, Super P, and poly(vinyl fluoride) (PVDF) binder at a weight ratio of 80:10:10. The mixture was pasted onto aluminum foil (Aldrich), and then dried in a vacuum oven at 120 °C for 12 h. Lithium foil (Aldrich) was used as the counter and reference electrode. Microporous PE film was used as the separator. The electrolyte was 1 M $LiPF_6$ in a mixture of EC and DEC (1:1, v/v, Merck). The $Li_4Ti_5O_{12}$/C composite batteries were charged by a constant + current at a constant voltage protocol (CC–CV), and discharged by a constant current profile, over a potential range of 0.5–2.5 V (vs. $Li/Li^+$) at various C rates, which were determined using a battery tester (Arbin BT2000). The second CV charge step of 3.80 V was terminated when the charged current was below 0.1 C. Cyclic voltammetry (CV) was performed using an Autolab instrument at a scanning rate of 0.1 mV $s^{-1}$, between 0.5 and 2.5 V (vs. $Li/Li^+$). The AC impedance spectroscopy was performed to obtain the AC spectra, using an Autolab PGSTAT302N potentiostat at a frequency range of 100 kHz–10 mHz, applying a 5 mV amplitude in an open circuit potential (OCP). All tests were performed at room temperature.

### 2.4. Electrochemical performance of the $Li_4Ti_5O_{12}/LiFePO_4$ full cell

The $LiFePO_4$/C cathode materials were prepared by a hydrothermal process and a post-sintering process [31]. The appropriate quantities of $FeSO_4 \cdot 7H_2O$, $LiOH \cdot H_2O$, and $NH_4H_2PO_4$ (Aldrich) as the starting materials were dissolved in 200 mL of deionized water. The Li:Fe:P molar ratio was 3:1:1. The polystyrene (PS, MW 35,000, Aldrich) polymer was dissolved in acetone to form a 5 wt.% PS stock solution. Approximately 50 mL of the 5 wt.% PS stock solution was added drop by drop into the polymer solution, while stirring. The added carbon source in the $LiFePO_4$ materials was maintained at 0–5 wt.%. The mixed solution was transferred into a

600 mL Teflon-lined stainless steel autoclave, which was heated at 170 °C for 15 h. After the solution had cooled to room temperature, the precipitate composite powder was cleaned and dried at 60 °C for 12 h in a vacuum oven, followed by post-sintering at 850 °C for 9 h under an $Ar/H_2$ (95:5, v/v) atmosphere. The $LiFePO_4$/C electrodes were prepared by mixing active $LiFePO_4$/C materials, Super P, and poly(vinyl fluoride) (PVDF) binder in a weight ratio of 80:10:10, pasted on aluminum foil (Aldrich), and then dried in a vacuum oven at 120 °C for 12 h. The as-prepared LTO was used as the counter electrode. A microporous PE film was used as the separator. The electrolyte was 1 M $LiPF_6$ in a mixture of EC and DEC (1:1, v/v, Merck). The $Li_4Ti_5O_{12}/LiFePO_4$ full cells were charged by a constant current + a constant voltage profile (CC–CV), and discharged by a constant current profile, over a potential range of 0.5–3.0 V at various C rates, determined using a battery tester (Arbin BT2000).

## 3. Results and discussion

Fig. 1(a) shows the XRD patterns of $Li_4Ti_5O_{12}$/C anode materials prepared using the solid-state method at various temperatures (700 °C, 800 °C, and 850 °C). The as-synthesized $Li_4Ti_5O_{12}$/C samples prepared at 700 °C and 800 °C contained some impurities, and their XRD peaks were not sharp, indicating poor crystallinity. By contrast, the XRD diffraction pattern of the $Li_4Ti_5O_{12}$/C composite material sintered at 850 °C contained no impurities, and was a single-phase material having a cubic spinel structure with an Fd-3m space group according to JCPDS File No. 26-1198. No other impurity peaks were found, demonstrating the high purity of the as-prepared $Li_4Ti_5O_{12}$/C composite sample prepared at 850 °C. The diffraction peak of the residual carbon could not be found in the pattern, suggesting low carbon content or an amorphous state. The lattice parameters of the as-prepared pure $Li_4Ti_5O_{12}$ sample and composite $Li_4Ti_5O_{12}$ sample were calculated based on the XRD patterns, and are listed in Table 1. The lattice parameters of the materials prepared using the solid-state method were 8.3597 Å and 8.3596 Å for $Li_4Ti_5O_{12}$ and $Li_4Ti_5O_{12}$/C, respectively. Additionally, it was found that the lattice parameters of all V-doped $Li_4Ti_5O_{12}$/C ($a$ = 8.35836 Å–8.35768 Å) cathode materials decreased with an increase in the concentration of vanadium (Table 1). The primary particle size of pristine LTO and all V-doped LTO/C samples is around 280.4–223.8 nm (based on XRD (111) peak) and the volume of units cell is around 585.564–584.252 $(Å)^3$. It was found that the 15%V-doped-LTO/C composite sample shows the smallest particle size and cell volume.

Fig. 1(b) shows the variation in the peak position of the (111) plane, which shifted to a higher angle direction. The XRD results show that the lattice parameters of all V-doped $Li_4Ti_5O_{12}$/C were smaller than that of $Li_4Ti_5O_{12}$, which can be explained by the fact that the ionic radius of $V^{5+}$ is the smallest of the 3 types of metallic ions in $Li_4Ti_5O_{12}$ (the ionic radius of $V^{5+}$ is 0.540 Å, $Ti^{4+}$ is 0.605 Å, and $Ti^{3+}$ is 0.670 Å) [22]. As a result, V was doped into the host structure of $Li_4Ti_5O_{12}$/C, and the lattice parameter decreased. In addition, the Furan resin, glucose, and PS polymer carbon sources had no observable influence on the structure of the $Li_4Ti_5O_{12}$/C composite materials (XRD data not shown).

Fig. 2(a)–(c) shows the SEM images of the pure $Li_4Ti_5O_{12}$, $Li_4Ti_5O_{12}$/C composite (5 wt.% Furan resin), and $Li_4Ti_{4.9}V_{0.1}O_{12}$/C samples prepared using the solid-state method. The particle size of the pure $Li_4Ti_5O_{12}$ sample ranged from 1 to 5 μm. By contrast, the particle sizes of the $Li_4Ti_5O_{12}$/C composite samples sintered at 850 °C decreased slightly (1–4 μm) when 5 wt.% Furan resin was added. The particle sizes of the V-doped $Li_4Ti_5O_{12}$/C composite samples sintered at 850 °C ranged from 1 to 3 μm. In general, the particle size increased when the sintering temperature was increased. Consequently, adding Furan resin as the carbon source not only decreased particle size, but also prevented the particles from growing during the sintering process. However, it appeared that the V-doping element did not affect the morphology of the V-doped $Li_4Ti_5O_{12}$/C composite samples.

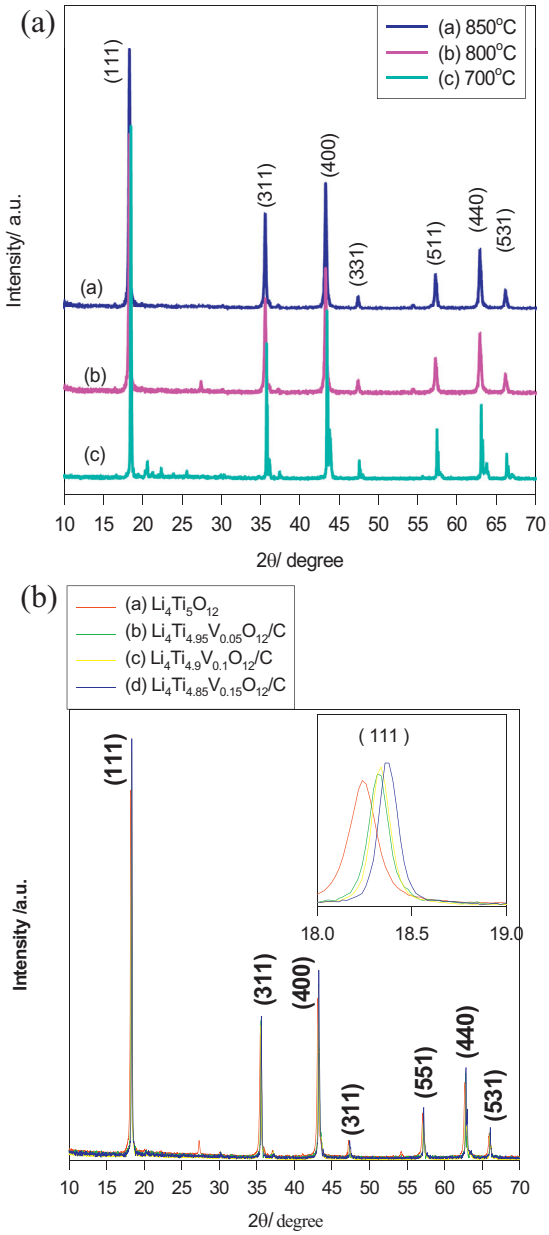


**Fig. 1.** XRD patterns of (a) $Li_4Ti_5O_{12}$/C at different temperatures; (b) $Li_4Ti_5O_{12}$/C with 5 wt.% Furan resin and different contents of V.

**Table 1**
The lattice parameters for $Li_4Ti_5O_{12}$/C cathode materials.

| Samples | Parameters | | |
|---|---|---|---|
| | $a$ (Å) | Volume $(Å^3)$ | $d$/nm based on XRD (111) peak |
| $Li_4Ti_5O_{12}$ | 8.35977 | 585.564 | 280.4 |
| $Li_4Ti_{4.95}V_{0.05}O_{12}$/5 wt.% Furan resin | 8.35836 | 584.906 | 263.7 |
| $Li_4Ti_{4.9}V_{0.1}O_{12}$/5 wt.% Furan resin | 8.35802 | 584.792 | 253.1 |
| $Li_4Ti_{4.85}V_{0.15}O_{12}$/5 wt.% Furan resin | 8.35768 | 584.252 | 223.8 |

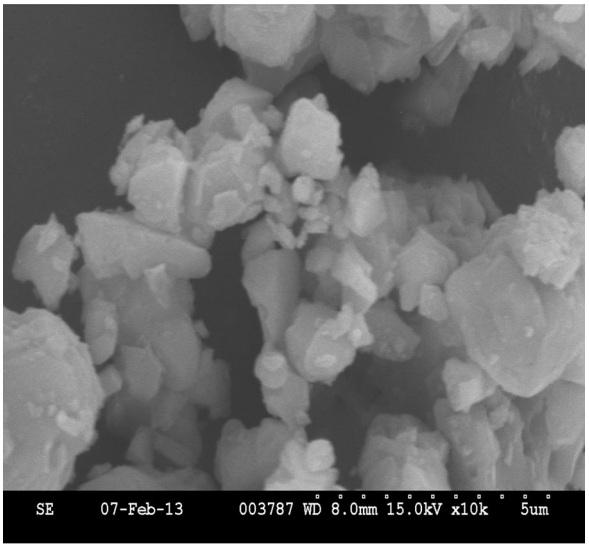


(a)

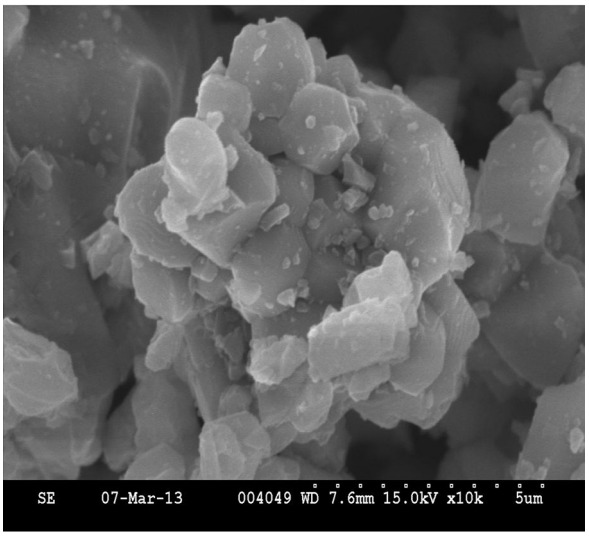


(b)

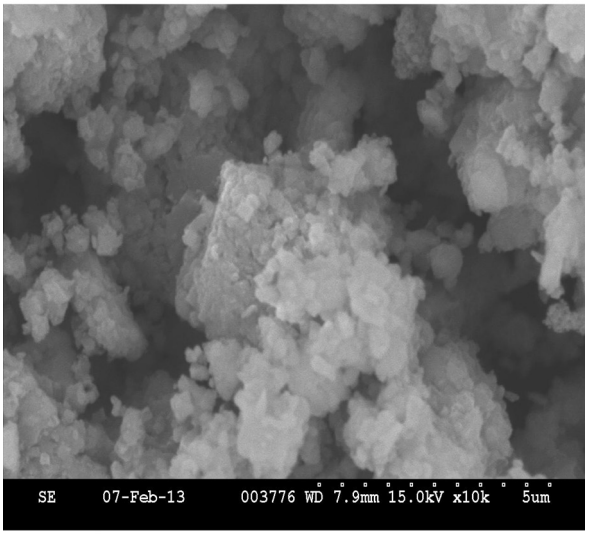


(c)

**Fig. 2.** SEM images of (a). pristine $Li_4Ti_5O_{12}$; (b). $Li_4Ti_5O_{12}$/C with 5 wt.% Furan resin; (c). 10%V-doped $Li_4Ti_5O_{12}$/C with 5 wt.% Furan resin.

The micro-Raman spectra of Pure LTO, *x*%V-doped LTO/C composite samples and $Li_4Ti_{4.90}V_{0.10}O_{12}$/C composite samples prepared at 850 °C are shown in Fig. 3(a) and (b), respectively. These samples displayed 5 Raman vibration peaks, at 217, 350, 428.3, 659, 1322, and 1590 $cm^{-1}$, as seen in Fig. 3(a) and (b). These Raman modes were in good agreement with the $A_{1g} + E_g + 3F_{2g}$ features of the spinel structure. The major micro-Raman peaks at 659 and 428.3 $cm^{-1}$ corresponded to the Ti–O and Li–O bond vibrations, respectively. The major peak at 217.4 $cm^{-1}$ corresponded to the bending vibration of the O–Ti–O bond. Furthermore, the Raman peak intensity decreased substantially in V-doped $Li_4Ti_5O_{12}$/C with respect to the un-doped samples, indicating that V doping resulted in an increased disordered state [20]. The Raman peak position corresponding to Li–O and Ti–O vibration position has a red-shift from 428.3 to 395.22 $cm^{-1}$ and from 659 to 658.5 $cm^{-1}$, respectively. The redshift of Raman peaks can be explained to the crystal. Clearly, The Li–O bond exhibits a more severe frequency shift than that of Ti–O bond. This phenomenon is correlated to with a weakening of the Li–O bond in V-doped LTO/C sample. Thus, The Li

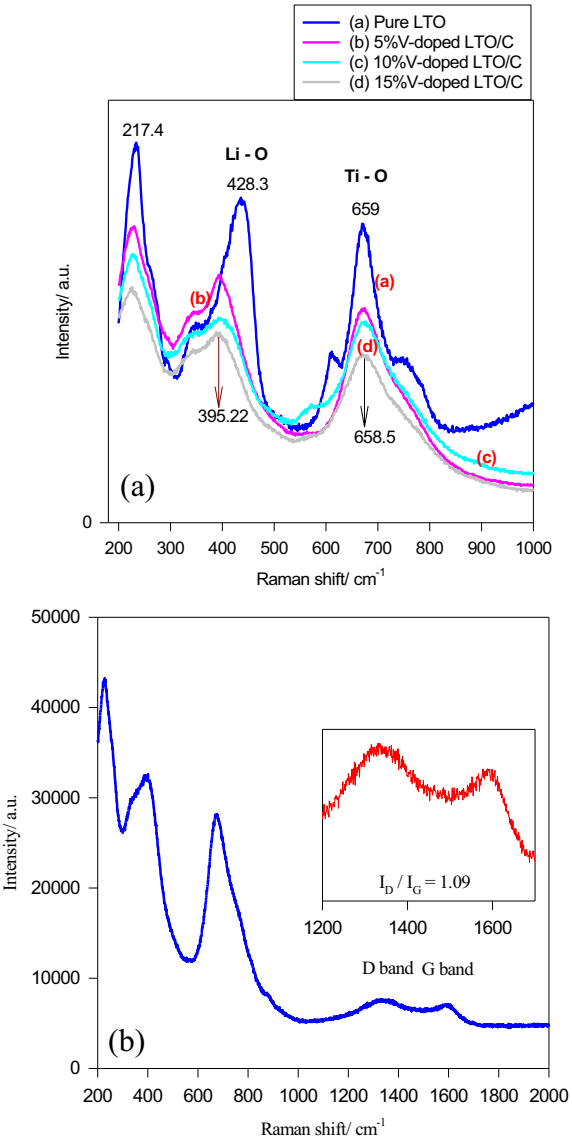


**Fig. 3.** Micro-Raman spectra of LTO and *x*%V-doped LTO/C anode composites; (b) $Li_4Ti_5O_{12}$/C composite samples with 5 wt.% Furan resin at 850 °C, respectively.

**Table 2**
The results of micro-Raman analysis for pure LTO and V-doped $Li_4Ti_5O_{12}$/C powders.

| Samples | Parameters |
|---|---|
| | $R$ ($=I_D/I_G$) ratio |
| $Li_4Ti_5O_{12}$/C (5% glucose) | 1.25 |
| $Li_4Ti_5O_{12}$/C (5% PS polymer) | 1.12 |
| $Li_4Ti_5O_{12}$/C (5% Furan resin) | 1.05 |
| $Li_4Ti_{4.95}V_{0.05}O_{12}$/C (5% Furan resin and doped 5%V) | 1.06 |
| $Li_4Ti_{4.9}V_{0.1}O_{12}$/C (5% Furan resin and doped 10%V) | 1.09 |
| $Li_4Ti_{4.85}V_{0.15}O_{12}$/C (5% Furan resin and doped 15%V) | 1.09 |
| Spherical $Li_4Ti_{4.9}V_{0.1}O_{12}$/C (5% Furan resin and doped 10%V, spray dry) | 1.02 |

ion diffusivity of V-doped LTO/C is much better than pristine LTO. In addition, the minor shift of Ti–O bond indicates that the structure stability of LTO can be retained after V-doped modification. Moreover, the Raman peak intensity of the 15% and 10%V-doped $Li_4Ti_5O_{12}$/C was lower than that of the 5%V-doped $Li_4Ti_5O_{12}$/C sample, which may be due to the enhanced contraction of the crystal lattice along the *a*-axis orientation, resulting from more V doping into $Li_4Ti_5O_{12}$.

Two additional Raman peaks of $Li_4Ti_{4.90}V_{0.10}O_{12}$/C composite sample was clearly observed at approximately 1322 and 1590 $cm^{-1}$; these peaks likely originated from the furan resin carbon source. The Raman peaks at 1322 $cm^{-1}$ (D-band) and 1590 $cm^{-1}$ (G-band) were not observed in the pure $Li_4Ti_5O_{12}$ sample. The broadening of the D ($A_{1g}$ symmetry) and G ($E_{2g}$ symmetry) bands, with a strong D band, indicated a localized in-plane $sp^2$ graphitic crystal domain, and a disordered $sp^3$ amorphous carbon. The intensity ratio of the D band vs. the G band (denoted as $R = I_D/I_G$) was used to estimate the carbon quality of the $Li_4Ti_5O_{12}$/C composite samples. The $R$ values of the $Li_4Ti_5O_{12}$/C composite samples prepared using Furan resin ($R$ = 1.05–1.09) were lower than those of the $Li_4Ti_5O_{12}$/C composite samples prepared using glucose ($R = 1.25$) or polystyrene polymer ($R = 1.12$). The $R$ values of the $Li_4Ti_5O_{12}$/C composite samples prepared with 5% Furan resin, glucose, and PS polymer carbon sources are also listed in Table 2 for comparison. The V-doped LTO/C composites prepared with various V-doping concentrations exhibited the same $R$ value (i.e., 1.06–1.09). It was reported that the discharge capacity and the rate capability of the $Li_4Ti_5O_{12}$/C composite samples were closely related to the intensity ratio of the D and G bands.

Table 3 lists several carbon-related properties of the $Li_4Ti_5O_{12}$/C composite samples, such as total residual carbon content and electronic conductivity. Both the electronic conductivity and the total residual carbon content were substantially affected by the discharge capacity and the rate capability of the $Li_4Ti_5O_{12}$/C composite anodes. The electronic conductivity of the pure $Li_4Ti_5O_{12}$ samples was approximately $1.34 \times 10^{-11}$ S $cm^{-1}$. This value was consistent with the data reported in the literature [11–15]. By

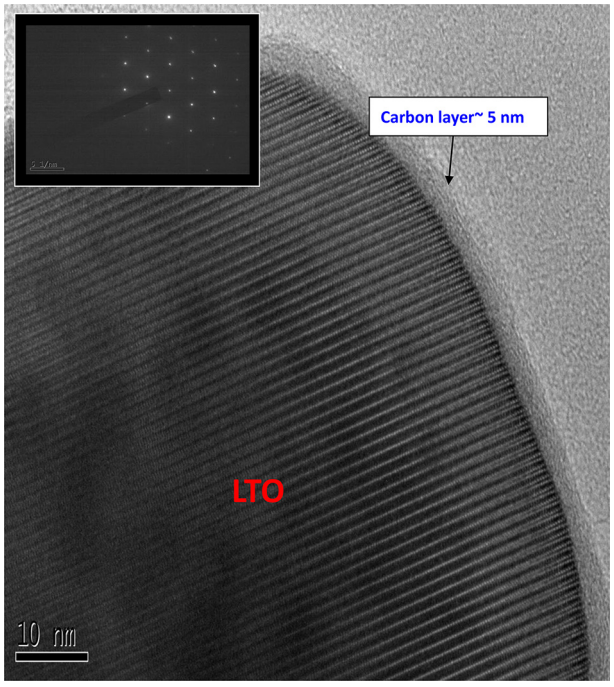


**Fig. 4.** TEM image of 10%V-doped $Li_4Ti_5O_{12}$/C material and the inset of SAED pattern.

contrast, the electronic conductivities of the $Li_4Ti_5O_{12}$/C composite samples to which 5 wt.% PS polymer, glucose, or furan resin were added as carbon sources were approximately $6.49 \times 10^{-7}$ S $cm^{-1}$, $1.49 \times 10^{-7}$ S $cm^{-1}$, and $5.34 \times 10^{-6}$ S $cm^{-1}$, respectively. The $Li_4Ti_5O_{12}$/C composite sample prepared with 5 wt.% Furan resin exhibited the highest conductivity. Moreover, the electronic conductivity of all V-doped $Li_4Ti_5O_{12}$/C composite samples prepared with 5 wt.% Furan resin was $4.8–7.2 \times 10^{-6}$ S $cm^{-1}$, as seen in Table 3. In addition, the residual carbon contents of all V-doped $Li_4Ti_5O_{12}$/C composite samples prepared with 5 wt.% Furan resin were 1.22%–1.43%. However, the residual carbon contents of the $Li_4Ti_5O_{12}$/C composite samples prepared with 5 wt.% glucose, PS polymer, or furan resin, were approximately 0.43%, 0.83%, and 1.22%, respectively. Based on these results, we prepared the LTO/C samples using furan resin as the major carbon source.

Fig. 4 shows the high-resolution TEM image of the 10%V-doped $Li_4Ti_5O_{12}$/C (or $Li_4Ti_{4.90}V_{0.10}O_{12}$/C) composite material. A 4 to 5-nm-thick amorphous carbon layer was uniformly coated on the $Li_4Ti_5O_{12}$ particle surface. The carbon layer on the composite sample was amorphous, but uniform. The amorphous carbon originated from the decomposition of the furan resin (the carbon source) on the surface of the $Li_4Ti_5O_{12}$ particles during the post-sintering process. The inset of Fig. 4 shows the selective area

**Table 3**
The results of residual carbon and electron conductivity of $Li_4Ti_5O_{12}$/C composites.

| Type | Data | | | | |
|---|---|---|---|---|---|
| | Weight/mg | | C% | | Conductivity/S $cm^{-1}$ |
| | Sample#1 | Sample#2 | Sample#1 | Sample#2 | |
| $Li_4Ti_5O_{12}$ | 1.76 | 2.12 | 0 | 0 | $1.34 \times 10^{-11}$ |
| $Li_4Ti_5O_{12}$/C with 5 wt.% glucose | 1.53 | 1.66 | 0.47 | 0.43 | $1.49 \times 10^{-7}$ |
| $Li_4Ti_5O_{12}$/C with 5 wt.% PS polymer | 1.78 | 1.92 | 0.82 | 0.84 | $6.49 \times 10^{-7}$ |
| $Li_4Ti_5O_{12}$/C with 5 wt.% Furan resin | 1.11 | 2.42 | 1.23 | 1.22 | $5.34 \times 10^{-6}$ |
| $Li_4Ti_{4.95}V_{0.05}O_{12}$/C with 5 wt.% Furan resin and 5 atomic%V | 2.41 | 2.59 | 1.36 | 1.37 | $4.80 \times 10^{-6}$ |
| $Li_4Ti_{4.9}V_{0.1}O_{12}$/C with 5 wt.% Furan resin and 10 atomic%V | 1.88 | 2.18 | 1.41 | 1.43 | $5.44 \times 10^{-6}$ |
| $Li_4Ti_{4.85}V_{0.15}O_{12}$/C with 5 wt.% Furan resin and 15 atomic%V | 1.98 | 1.59 | 1.39 | 1.40 | $7.20 \times 10^{-6}$ |

**Table 4**
The chemical composition of V-doped $Li_4Ti_5O_{12}$/C by XRF.

| Samples | Parameters | | | |
|---|---|---|---|---|
| | Element | Weight percent/% | Mole | Mole ratio |
| $Li_4Ti_{4.95}V_{0.05}O_{12}$/C (doped 5%V) | Ti | 98.935 | 2.06 | 4.95 |
| | V | 1.065 | 0.021 | 0.05 |
| $Li_4Ti_{4.85}V_{0.10}O_{12}$/C (doped 10%V) | Ti | 97.718 | 2.0414 | 4.90 |
| | V | 2.282 | 0.0447 | 0.107 |
| $Li_4Ti_{4.85}V_{0.15}O_{12}$/C (doped 15%V) | Ti | 96.501 | 2.0159 | 4.85 |
| | V | 3.409 | 0.0686 | 0.16 |

electron diffraction (SAED) pattern, indicating a well-crystallized structure and no other crystalline phases present, except for the spinel phase. The particles of the $Li_4Ti_5O_{12}$/C composite materials prepared using 5 wt.% Furan resin had a higher residual carbon content (C%: 1.2–1.4%) than those of the materials prepared using other carbon sources, namely glucose and PS polymer (C% was less than 1%).

The V-doped composition of the V-doped $Li_4Ti_5O_{12}$/C composite was examined by XRF. Table 4 lists the results of the analysis of all V-doped LTO/C composites, indicating that the nominal V content was close to the real V content in the composite.

Fig. 5 shows the initial charge/discharge profiles of $Li_4Ti_5O_{12}$/C prepared with 5 wt.% Furan resin, 5%V-doped $Li_4Ti_5O_{12}$/C, 10%V-doped $Li_4Ti_5O_{12}$/C, and 15%V-doped $Li_4Ti_5O_{12}$/C composite samples calcined at 850 °C at a 0.1C rate in the potential range of 0.5–2.5 V. The discharge capacities of the 0%, 5%, 10% and 15%V-doped $Li_4Ti_5O_{12}$/C samples were 158.72, 173.19, 179.80, and 181.25 mAh $g^{-1}$. It was found that the discharge capacities of the 10% and 15%V-doped LTO/C sample are over 175 mAh $g^{-1}$ (theoretical reversible capacity in 1–2.5 V only 175 mAh $g^{-1}$) in the potential range of 0.5–2.5 V. The V-doped $Li_4Ti_5O_{12}$/C composite exhibited a flat discharge plateau at 1.55 V (vs. $Li/Li^+$). However, the $Li_4Ti_5O_{12}$/C samples (without any V doping) showed a sloping charge behavior when the charge voltage decreased to 0.50 V (vs. $Li/Li^+$). The 5%V-doped and 15%V-doped $Li_4Ti_5O_{12}$/C composites—but not the 10%V-doped $Li_4Ti_5O_{12}$/C composite—also showed a sloping charge behavior. The reason for the sloping charge behavior may be due to the poor electrical conductivity and the low ionic diffusion coefficient. The electrochemical performance of the 10%V-doped $Li_4Ti_5O_{12}$/C composite was superior to those of the 5%V-doped and 15%V-doped $Li_4Ti_5O_{12}$/C composites.

The inset of Fig. 5 also shows the cyclic voltammetry (CV) of the $Li_4Ti_{4.90}V_{0.10}O_{12}$/C sample in the first cycle at a scan rate of 0.1 mV $s^{-1}$ within a potential window of 0.5–2.5 V (vs. $Li/Li^+$). The first oxidation and reduction pair peaks of the $Li_4Ti_5O_{12}$/C composite appeared at approximately 1.684 and 1.464 V, respectively, and the potential difference between the two peaks was 0.220 V. There is also a second pair peak around 0.5–0.75 V. The first insertion process with a flat plateau of 1.55 V corresponds to the two phase insertion process between $Li_4Ti_5O_{12}$ and $Li_7Ti_5O_{12}$, in which three lithium ions insertion into LTO accompany with three $Ti^{4+}$ are reduced to $Ti^{3+}$; namely, the octahedral (16c) sites of are occupied by lithium ions. The electrochemical reaction can be ascribed as Eq. (1) [21]:

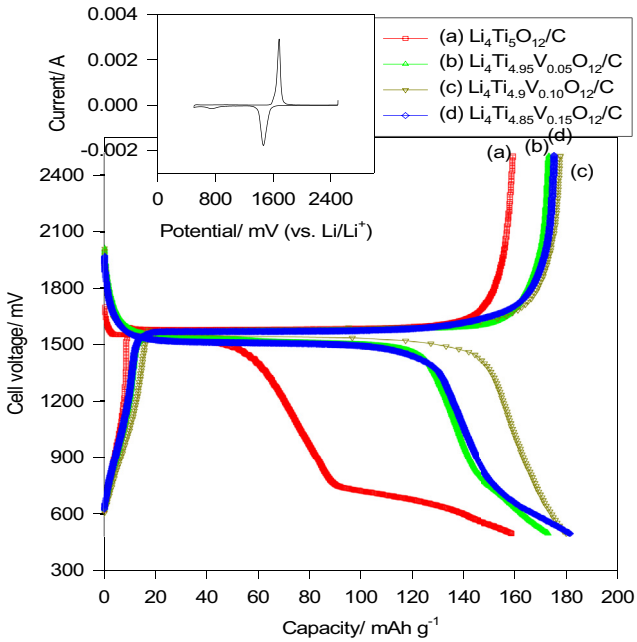


**Fig. 5.** The initial charge–discharge curves for (a). LTO/C and *x*%V-doped $Li_4Ti_5O_{12}$/C samples at 850 °C at 0.1C/0.1C rate in the potential range of 0.5 V–2.5 V; the inset for CV curve 10%V doped LTO/C in the potential range of 0.5V–2.5 V.

$$Li_{3(8a)}\left[LiTi_5^{4+}\right]_{(16d)}O_{12(32e)} + 3Li^+ + 3e^- \rightarrow Li_{6(16c)}\left[LiTi_3^{3+}Ti_2^{4+}\right]_{(16d)}O_{12(32e)} \quad (1)$$

However, there are still two $Ti^{4+}$ remaining in $Li_7Ti_5O_{12}$, which can be further reduced below 0.75 V without octahedral sites (16c) available. When we decrease the charge voltage, the appearance of the sloping regions indicates the second electrochemical insertion process (our work below 0.75 V) occurred. The tetrahedral (8a) sites of can accommodate lithium ions in the voltage window of 0.75–0.01 V. The second insertion lithium ion process can be described as:

$$Li_{6(16c)}\left[LiTi_3^{3+}Ti_2^{4+}\right]_{(16d)}O_{12(32e)} + 2Li^+ + 2e^- \rightarrow Li_{2(8a)}Li_{6(16c)}\left[LiTi_5^{3+}\right]_{(16d)}O_{12(32e)} \quad (2)$$

The charge voltage range for our V-doped LTO/C composite sample is only in 0.5–2.5 V range in order to avoid the reduction of electrolyte on the anode surface and the formation of the solid-electrolyte interphase (SEI); moreover, the reversible capacity can be obtained can be over 175 mAh $g^{-1}$.

Fig. 6 displays the typical charge/discharge curves of the 10%V-doped $Li_4Ti_5O_{12}$/C samples prepared at 850 °C, at various rates (i.e., at 0.2C/0.2C, 0.2C/0.5C, 0.2C/1C, 0.2C/3C, 0.2C/5C, 0.2C/10C, and 0.2C/20C). All $Li_4Ti_5O_{12}$ samples revealed the typical flat potential plateau at 0.5–2.5 V (vs. $Li/Li^+$). The 10%V-doped $Li_4Ti_5O_{12}$/C composite sample delivered specific discharge capacities of 170.59, 168.53, 165.59, 150.29, 130.44, 110.15, and 76.76 mAh $g^{-1}$ at rates of 0.2, 0.5, 1, 3, 5, 10, and 20C, respectively. However, the $Li_4Ti_5O_{12}$/C

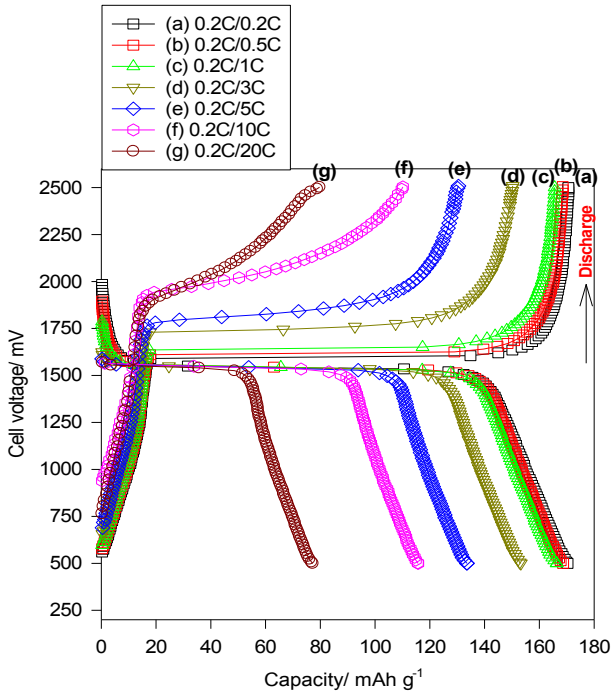


**Fig. 6.** The 10%V doped $Li_4Ti_5O_{12}$/C samples at 850 °C at 0.2C/0.2C–10C rates (All curves in the potential range of 0.5 V–2.5 V).

composite sample (i.e., without any V doping) delivered specific discharge capacities of 93.92, 83.61, 74.43, 46.91, 35.67, 17.42, and 2.03 mAh $g^{-1}$ at discharge rates of 0.2, 0.5, 1, 3, 5, 10, and 20C, respectively (data not shown). Moreover, the 15%V-doped $Li_4Ti_5O_{12}$/C composite sample delivered specific discharge capacities of 183.97, 176.91, 159.16, 141.83, 130.13, 67.31, and 1.10 mAh $g^{-1}$ at rates of 0.2, 0.5, 1, 3, 5, 10, and 20C, respectively (data not shown). When we used 5 wt.% Furan resin as the carbon source, and selected a 10%V doping in LTO, the resulting 10%V-doped LTO/C composite materials showed the highest discharge capacity (76.76 mAh $g^{-1}$ at a 20C rate at room temperature) and the most efficient performance among the four LTO/C anode materials. However, the 15%V-doped LTO/C composite materials showed the highest discharge capacity (183.97 mAh $g^{-1}$ at a 0.1C rate at room temperature) and the most efficient performance among three V-doped LTO materials. Yu et al. [22] studied the electrochemical properties of a $Li_4Ti_{4.9}V_{0.1}O_{12}$/C anode material prepared using a solid-state method. They showed that the discharge capacities were as high as 166 mAh $g^{-1}$ at 0.5C and 117.3 mAh $g^{-1}$ at 5C. By comparison, our V-doped LTO/C anode material exhibited a superior electrochemical performance (168.53 mAh $g^{-1}$ at 0.5C and 130.44 mAh $g^{-1}$ at 5C), as compared with their materials.

Our results further revealed that the highest specific discharge capacity of the $Li_4Ti_5O_{12}$/C composite materials containing 3.29% residual carbon at a 0.1C rate was 163 mAh $g^{-1}$, and their coulombic efficiency was 98–99%. However, the specific discharge capacity and the coulombic efficiency at a 1C rate were 135 mAh $g^{-1}$ and 95%, respectively. A sol–gel process was also used to synthesize $Li_4Ti_5O_{12}$/C composite cathode materials for comparison. For this process, citric acid was used as a reducing agent. The highest residual carbon content of the $Li_4Ti_5O_{12}$/C composite material with CA:1.0, sintered at 750 °C, was approximately 11.94 wt.%. The optimal sintering temperature for the sol–gel process was 750 °C. The highest specific discharge capacity of the $Li_4Ti_5O_{12}$/C composite prepared using a sol–gel process at a 0.1C rate was 130 mAh $g^{-1}$, and its coulombic efficiency was 98%. However, the specific discharge capacity and the coulombic efficiency at a 3C rate were only 80 mAh $g^{-1}$ and 95%, respectively.

The rate capability performances of the LTO/C, and 5%, 10%, and 15%V-doped $Li_4Ti_5O_{12}$/C composite samples at various rates from 0.2 to 20C are presented in Fig. 7 for comparison. The $Li_4Ti_5O_{12}$/C composite samples exhibited poor high-rate performances because they were unable to maintain charge/discharge rate of 20C. By contrast, the 10%V-doped $Li_4Ti_5O_{12}$/C composite exhibited the optimal rate performance among the four composite materials. It was found that the 10%V-doped $Li_4Ti_5O_{12}$/C composite sample exhibited an excellent high-rate performance of performance, as shown in Fig. 7, the discharge capacities at 10C and 20C are approximately 118 and 79 mAh $g^{-1}$, respectively. However, the electrochemical performance of the 15%V-doped $Li_4Ti_5O_{12}$/C composite sample still exhibited good performance only at rates of 0.2C–5C. The 15%V-doped $Li_4Ti_5O_{12}$/C composite sample showed poor performance at 10–20C rate, indicating that the discharge capacities at 10C and 20C are only 67 and 32 mAh $g^{-1}$, respectively. This result may be due to the crystal distortion generated by adding a large amount of V to LTO during doping.

The AC impedance spectroscopy was used to study the interface properties of the $Li_4Ti_5O_{12}$/C composite samples. Fig. 8(a) shows the AC spectra of the $Li_4Ti_5O_{12}$/C composite, and 5%, 10%, and 15%V-doped $Li_4Ti_5O_{12}$/C composite samples at open circuit potential. Each AC plot consisted of one semicircle at high frequency, followed by a linear portion at low frequency. The low-frequency region of the straight line was considered to be Warburg impedance, which is for long-range Li-ion diffusion in bulk phase. The equivalent circuit is shown in the inset of Fig. 8(b); $R_b$ indicates the bulk resistance to the electrolyte, $R_{ct}$ is the charge transfer resistance at the active material interface, and CPE represents the double-layer capacitance and some surface film capacitance. The Li chemical diffusion coefficients of the electrode were calculated based on Eq. (3) [15–17].

$$D_i = \frac{1}{2}\left(\frac{RT}{AF^2\sigma C}\right)^2 \quad (3)$$

where $\sigma$ is the Warburg impedance coefficient (obtained as a slope from a plot of $Z_{re}$ vs. $\varpi^{-0.5}$, as seen in Fig. 8(b)), $D_i$ is the lithium diffusion coefficient, $R$ is the gas constant, $T$ is the absolute

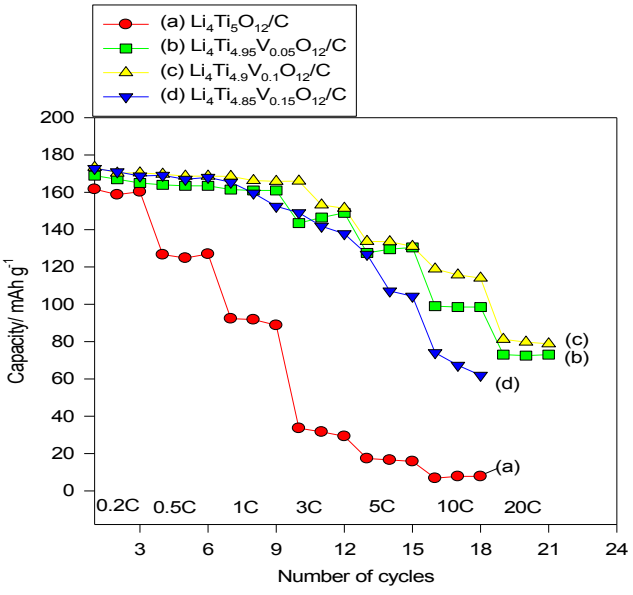


**Fig. 7.** The rate performances of LTO/C and *x*%V-doped $Li_4Ti_5O_{12}$/C electrodes.

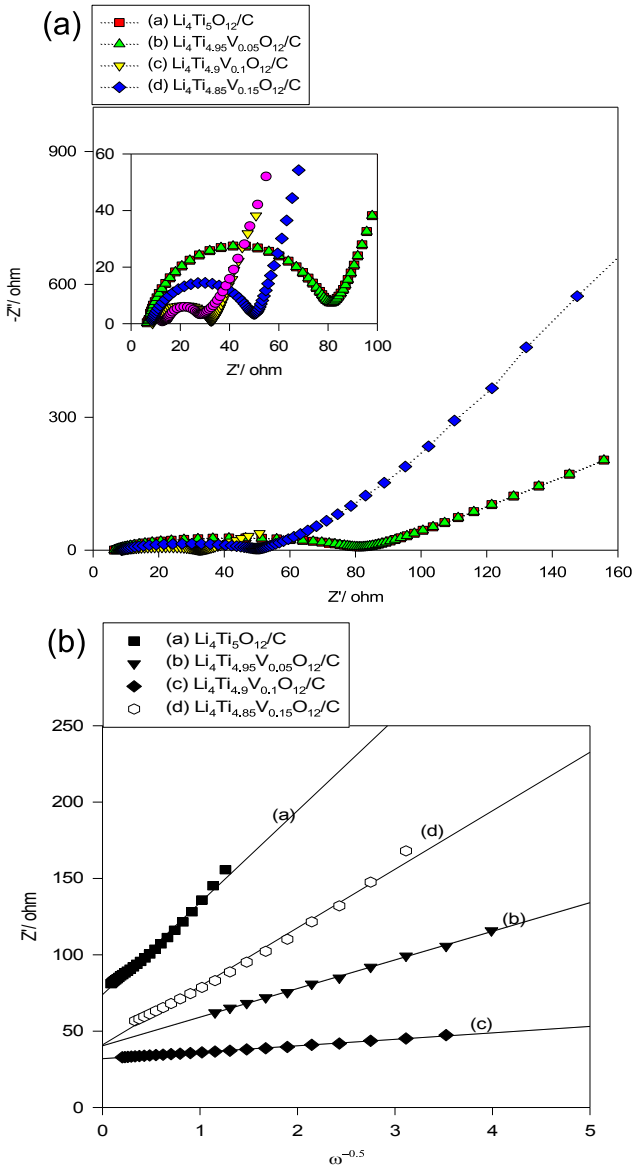


**Fig. 8.** (a) Nyquist plot of *x*%V-doped $Li_4Ti_5O_{12}$/C electrodes at 850 °C. at OCP; (b) the relationship between Z′ and the inverse square root of frequency ($\omega^{-1/2}$) in the frequency range.

temperature, *F* is Faraday's constant, *A* is the area of the electrode, and C is the molar concentration of $Li^+$ ions ($C_{Li}$ = 4.37 × $10^{-3}$ mol $cm^{-3}$) [32,33]. Table 5 summarizes the calculated $R_b$, $R_{ct}$, $D_i$, and $j_o$ parameters for the LTO/C, and V-doped LTO/C composite samples. The $R_b$ values of LTO/C and all V-doped LTO/C were 6–8 Ω, but that of the pure LTO sample was 4 Ω. The $R_{ct}$ and $D_i$ values of the composite samples varied considerably. After V doping and carbon coating, the charge resistance values and Li diffusion coefficients were improved, enhancing the rate capability of the LTO anode materials. The $j_o$ value indicates the reaction kinetic of the LTO materials, and can be obtained as follows: $j_o = RT/nFR_{ct}$. The pure LTO sample exhibited the highest $R_{ct}$ value (98.69 Ω), but the lowest Li diffusion coefficient ($D_i$; 4.25 × $10^{-15}$ $cm^2$ $s^{-1}$) and the lowest $j_o$ value (1.96 × $10^{-4}$ A $cm^{-2}$). The 10%V-doped $Li_4Ti_5O_{12}$/C composite sample exhibited the lowest $R_{ct}$ value (25.50 Ω), but the highest Li diffusion coefficient ($D_i$; 2.84 × $10^{-11}$ $cm^2$ $s^{-1}$) and the highest $j_o$ value (7.59 × $10^{-4}$ A $cm^{-2}$). As a result, carbon coating and V doping were applied to the LTO anode material to enhance both its electrochemical performance and rate capability. Yu et al. [22] reported that the Li diffusion coefficient ($D_i$) of pure LTO was approximately 2.70 × $10^{-15}$ $cm^2$ $s^{-1}$, which is close to our result (4.25 × $10^{-15}$ $cm^2$ $s^{-1}$, obtained using the AC impedance method). However, they reported that the Li diffusion coefficient ($D_i$) of the $Li_4Ti_{4.9}V_{0.1}O_{12}$ composite sample was approximately 6.5 × $10^{-13}$ $cm^2$ $s^{-1}$, which is much lower than our result (2.84 × $10^{-11}$ $cm^2$ $s^{-1}$, obtained using the AC impedance method).

Fig. 9(a) shows the three initial charge/discharge profiles of the $LiFePO_4$/Li composite cells at a 0.1C rate at 25 °C. The $LiFePO_4$/C composite exhibited a flat discharge plateau at 3.30 V (vs. Li/$Li^+$). The $LiFePO_4$/Li half-cells based on $LiFePO_4$/C as-synthesized materials delivered a specific capacity of 160 mAh $g^{-1}$ at a 0.1C rate. The typical charge/discharge profiles of the $LiFePO_4$/Li half-cell at various rates from 0.2 to 10C are displayed in Fig. 9(b). The $LiFePO_4$/Li cell also exhibited a typically flat potential plateau at 3.4–3.5 V (vs. Li/$Li^+$) at 0.1C. The LFP sample delivered specific capacities of 142, 139, 128, 108, and 93 mAh $g^{-1}$ at rates of 0.2, 0.5, 1, 3, and 5C, respectively.

**Table 5**
The AC impedance parameters, lithium diffusion coefficient, and exchange current density values of $Li_4Ti_5O_{12}$ samples.

| Samples | Parameters | | | | |
|---|---|---|---|---|---|
| | $R_b$/Ω | $R_{ct}$/Ω | σ | $D_{Li+}$/$cm^2$ $s^{-1}$ | $j_o$/A $cm^{-2}$ |
| $Li_4Ti_5O_{12}$/C (0%V) | 7.07 | 74.61 | 60.24 | 1.45 × $10^{-13}$ | 2.61 × $10^{-4}$ |
| $Li_4Ti_{4.95}V_{0.05}O_{12}$/C (5%V) | 6.05 | 38.40 | 18.74 | 1.49 × $10^{-12}$ | 5.03 × $10^{-4}$ |
| $Li_4Ti_{4.9}V_{0.1}O_{12}$/C (10%V) | 8.10 | 25.50 | 4.30 | 2.84 × $10^{-11}$ | 7.59 × $10^{-4}$ |
| $Li_4Ti_{4.85}V_{0.15}O_{12}$/C (15%V) | 8.52 | 44.50 | 1.65 | 1.93 × $10^{-10}$ | 4.34 × $10^{-4}$ |

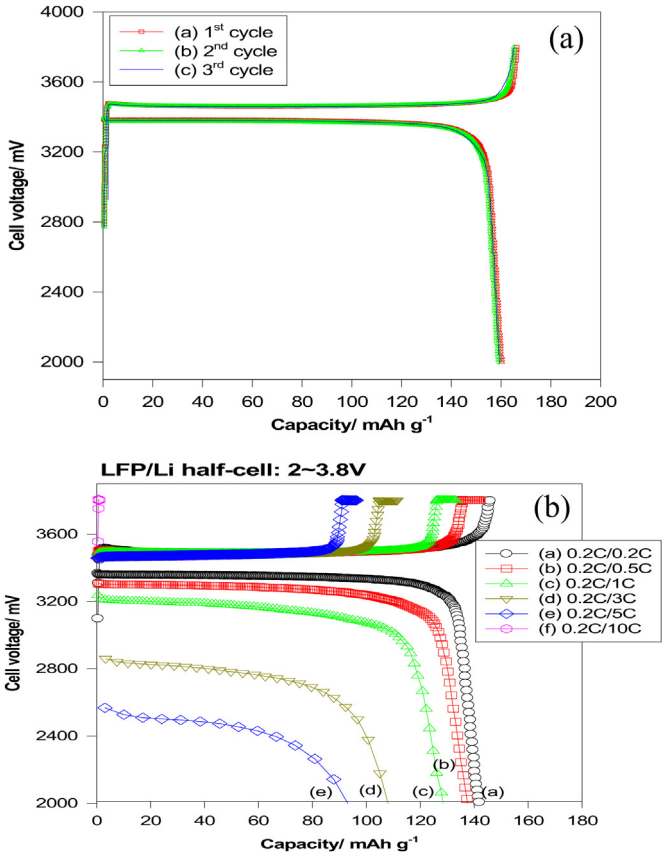


**Fig. 9.** The charge/discharge curve of $LiFePO_4$/C half cell: (a) 0.1C; (b) 0.2–10C rate.

Fig. 10(a) shows the initial five charge/discharge curves of the $Li_4Ti_5O_{12}$/$LiFePO_4$ full cell at a 0.1C rate at 25 °C. The $Li_4Ti_5O_{12}$/$LiFePO_4$ cell exhibited a flat discharge plateau at 1.85 V. The $Li_4Ti_5O_{12}$/$LiFePO_4$ full cells based on the as-synthesized LTO anode and LFO cathode materials delivered a specific capacity of approximately 184 mAh $g^{-1}$ at a 0.1C rate. The typical charge/discharge profiles of the $Li_4Ti_5O_{12}$/$LiFePO_4$ full cell at various rates from 0.2 to 10C are displayed in Fig. 10(b). The $Li_4Ti_5O_{12}$/$LiFePO_4$ full cell exhibited a varied potential plateau at 1.5–1.8 V (vs. Li/$Li^+$). The $Li_4Ti_5O_{12}$/$LiFePO_4$ battery delivered specific capacities of 181, 178, 167, 142, 110, and 78 mAh $g^{-1}$ at rates of 0.2, 0.5, 1, 3, 5, and 10C, respectively. Morales et al. [28] examined the electrochemical behavior of Li-ion batteries, namely LiAl/$LiFePO_4$, Al/$LiFePO_4$, and $Li_4Ti_5O_{12}$/$LiFePO_4$. The LTO/$LiFePO_4$ full cell exhibited the most efficient performance among the three cells. The $Li_4Ti_5O_{12}$/$LiFePO_4$ cells provided capacities of approximately 150 mAh $g^{-1}$ at 1C in the 100th cycle. Therefore, the performance of our $Li_4Ti_5O_{12}$/$LiFePO_4$ cell at a 1C rate (167 mAh $g^{-1}$) was superior to that of their $Li_4Ti_5O_{12}$/$LiFePO_4$ cell (150 mAh $g^{-1}$).

Fig. 11 shows the cycle-life performance of the $Li_4Ti_5O_{12}$/$LiFePO_4$ full cell for 400 cycles at a 1C charge and 3C discharge rate. The cell exhibited excellent cycle charge/discharge stability without any fading after a 400-cycle test. Nevertheless, the discharge capacity declined from 139.1 to 136 mAh $g^{-1}$ after a 400 cycle test. The fading rate was approximately 0.0056% per cycle. The capacity retention was approximately 98.1%. Morales et al. [28] also studied the long-term and high-rate performance of $Li_4Ti_5O_{12}$/$LiFePO_4$ cells. They determined discharge capacities of 160, 150, 125, and 110 mAh $g^{-1}$ at rates of 0.1, 1, 4, and 8C, respectively. The fading rate of the full cell was approximately 0.01% per cycle after 2500 cycles. In contrast with the cell developed by Morales et al., our as-synthesized cell exhibited an optimal high-rate capability (up to 10C) and excellent long-term stability (i.e., lower fading rate (0.0056% per cycle)). The inset of Fig. 11 also shows the AC impedance spectra of the $Li_4Ti_5O_{12}$/$LiFePO_4$ full cell after a 400-cycle test, indicating a stable and small charge transfer resistance of approximately 190 Ω. The cell voltage difference of the charge and discharge plateau was approximately 380 mV. As a result, the V-doped LTO anode material can be considered an outstanding candidate for high-power Li-ion battery applications.

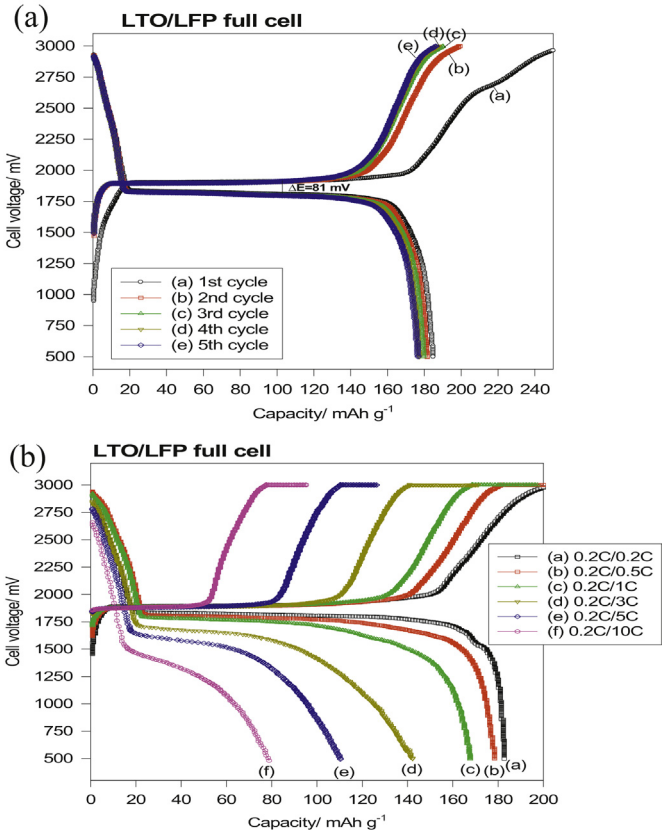


**Fig. 10.** The charge/discharge curve of $LiFePO_4$/LTO full cell: (a) 0.1C; (b) 0.2–10C rates.

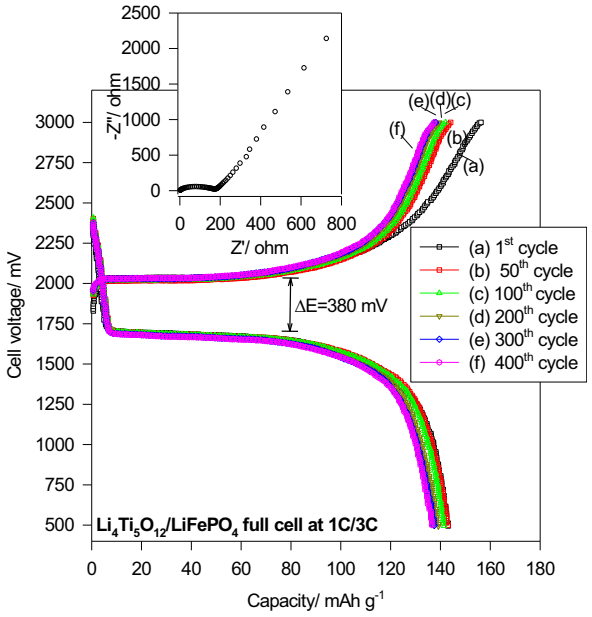


**Fig. 11.** The charge/discharge curve of LTO/LFP full cell at 1C charge and 3C discharge rate; the inset for AC impedance spectra of the full cell at OCP.

## 4. Conclusion

We prepared a novel $Li_4Ti_5O_{12}$/C composite material, using a solid-state method. By doping vanadium (V) and coating carbon on the $Li_4Ti_5O_{12}$ material, the rate capability and cycle stability were substantially enhanced. Furan polymer was the most promising carbon source, compared with glucose and polystyrene polymer. The characteristic properties of the materials were examined by X-ray diffraction (XRD), micro-Raman, scanning electron microscopy (SEM), AC impedance method, and galvanostatic charge/discharge method. We also prepared $Li_4Ti_5O_{12}$/C composite materials with and without V doping for comparison. As a result, the $Li_4Ti_{4.90}V_{0.10}O_{12}$/C composite material achieved optimal discharge capacities of 169 and 73 mAh $g^{-1}$ at a 1C/1C and 20C/20C rate, respectively. We constructed and evaluated the $Li_4Ti_5O_{12}$/$LiFePO_4$ full cell and the capacity is limited by LTO anode. The full cell exhibited discharge capacities of 178.45, 167.67, 142.24, 110.34, and 78.88 mAh $g^{-1}$ at 0.5, 1, 3, 5, and 10C, respectively. Compared with other cells, the LTO/LFP full cell exhibited a superior high-rate capability up to 10C and excellent long-term stability with a lower fading rate of 0.0056% per cycle. Our work demonstrated that the $Li_4Ti_{4.95}V_{0.05}O_{12}$/C composite can be considered an outstanding candidate for application in Li-ion batteries as anode materials.

## Acknowledgments

Financial support from the National Science Council, Taiwan (Project No: NSC 101-2221-E-131-037) is gratefully acknowledged.

## References


[1] R. Fong, U. Sacken, J.R. Dahn, J. Electrochem. Soc. 137 (1990) 2009–2013.
[2] H. Fujimoto, A. Mabuchi, K. Tokumitsu, T. Kasuh, J. Power Sources 54 (1995) 440–443.
[3] X. Qiu, Q. Liu, L. Yang, Solid State Ionics 60 (1993) 351–355.
[4] T. Ohzuku, A. Ueda, N. Yamamoto, J. Electrochem. Soc. 142 (1995) 1431–1435.
[5] S. Scharner, W. Weppner, P. Schmid-Beurmann, J. Electrochem. Soc. 146 (1999) 857–861.
[6] Y.R. Zhu, L.C. Yin, T.F. Yi, H. Liu, Y. Xie, R.S. Zhu, J. Alloys Compd. 547 (2013) 107–112.
[7] T.F. Yi, H. Liu, Y.R. Zhu, L.J. Jiang, Y. X, R.S. Zhu, Y. Xie, R.S. Zhu, J. Power Sources 215 (2012) 258–265.
[8] Y. Tang, Li Yang, S. Fang, Z. Qiu, Electrochim. Acta 54 (2009) 6244–6249.
[9] H. Xiang, B. Tian, P. Lian, Z. Li, H. Wang, J. Alloys Compd. 509 (2011) 7205–7209.
[10] X. Hu, Z. Lin, K. Yang, Y. Huai, Z. Deng, Electrochim. Acta 56 (2011) 5046–5053.
[11] T. Ogihara, M. Yamada, A. Fujita, S. Akao, K. Myoujin, Mater. Res. Bull. 46 (2011) 796–800.
[12] H.G. Jung, J. Kim, B. Scrosati, Y.K. Sun, J. Power Sources 196 (2011) 7763–7766.
[13] X. Li, M. Qu, Y. Huai, Z. Yu, Electrochim. Acta 55 (2010) 2979–2982.
[14] J. Wang, X.M. Liu, H. Yang, X.D. Shen, J. Alloys Compd. 509 (2011) 712–718.
[15] P. Kubiak, A. Garcia, M. Womes, L. Aldon, J. Olivier-Fourcade, P.E. Lippens, J.C. Jumas, J. Power Sources 121 (2003) 626–630.
[16] H. Zhao, Y. Li, Z. Zhu, J. Lin, Z. Tian, R. Wang, Electrochim. Acta 53 (2008) 7079–7083.
[17] S. Ji, J. Zhang, W. Wang, Y. Huang, Z. Feng, Z. Zhang, Z. Tang, Mater. Chem. Phys. 123 (2010) 510–515.
[18] B. Tian, H. Xiang, L. Zhang, Z. Li, H. Wang, Electrochim. Acta 55 (2010) 5453–5458.
[19] F. Gu, G. Chen, Z. Wang, J. Solid State Electrochem. 16 (2012) 375–382.
[20] Y.-R. Jhan, J.-G. Duh, Electrochim. Acta 63 (2012) 9–15.
[21] D. Ahn, X. Xiao, Electrochem. Commun. 13 (2011) 796–799.
[22] Z. Yu, X. Zhang, G. Yang, J. Liu, J. Wang, R. Wang, Electrochim. Acta 56 (2011) 8611–86175.
[23] T.F. Yi, J. Shu, Y.-R. Zhu, X.-D. Zhu, R.-S. Zhu, A.-N. Zhou, J. Power Sources 195 (2010) 285–288.
[24] T.F. Yi, S.Y. Yang, X.Y. Li, J.H. Yao, Y.R. Zhu, R.S. Zhu, J. Power Sources 246 (2014) 505–511.
[25] Z. Zhang, L. Cao, J. Huang, S. Zhou, Y. Huang, Y. Cai, Ceram. Int. 39 (2013) 6139–6143.
[26] J. Gao, J. Ying, C. Jiang, C. Wan, Ionics 15 (2009) 597–601.
[27] T.F. Yi, Y. Xie, L.J. Jiang, J. Shu, C.B. Yue, A.N. Zhou, M.F. Ye, RSC Adv. 2 (2012) 3541–3547.
[28] J. Morales, R. Trocoli, S. Franger, J. Santos-Pena, Electrochim. Acta 55 (2010) 3075–3082.
[29] X. Guo, H.F. Xiang, T.P. Zhou, W.H. Li, X.W. Wang, J.X. Zhou, Y. Yu, Electrochim. Acta 109 (2013) 33–38.
[30] H.F. Xiang, X. Zhang, Q.Y. Jin, C.P. Zhang, C.H. Chen, X.W. Ge, J. Power Sources 183 (2008) 355–360.
[31] C.C. Yang, Y.C. Chen, Y.C. Liao, Mater. Res. Bull. 47 (2012), 2616–2622.
[32] T.F. Yi, Y. Xie, Q. Wu, H. Liu, L. Jiang, M. Ye, R. Zhu, J. Power Sources 214 (2012) 220–226.
[33] S.L. Chou, J.Z. Wang, H.K. Liu, S.X. Dou, J. Phys. Chem. C 115 (2011) 16220–16227.